

Electron-phonon Vertex in the Two-dimensional One-band Hubbard Model

Z. B. Huang, W. Hanke, and E. Arrigoni

Institut für Theoretische Physik, Universität Würzburg, am Hubland, 97074 Würzburg, Germany

D. J. Scalapino

Department of Physics, University of California, Santa Barbara, California 93106-9530 USA

(Dated: October 28, 2019)

Using Quantum Monte Carlo techniques, we study the effects of electronic correlations on the effective electron-phonon (el-ph) coupling in a two-dimensional one-band Hubbard model. We consider a momentum-independent bare ionic el-ph coupling. In the weak- and intermediate-coupling regimes, we find that the on-site Coulomb interaction U acts to effectively suppress the ionic el-ph coupling at all electron- and phonon- momenta. In this regime, our numerical simulations are in good agreement with the results of perturbation theory to order U^2 . However, entering the strong-coupling regime, we find that the forward scattering process stops decreasing and begins to increase as a function of U , leading to an effective el-ph coupling which is peaked in the forward direction. This increase comes from the irreducible vertex corrections, which depend crucially on the renormalized electronic structure of the strongly correlated system.

The role of the el-ph interaction in the physics of the high T_c cuprate superconductors remains unclear. On the one hand, the linear T dependence of the resistivity up to high temperatures and the small value of the isotope coefficient of the optimally doped materials suggest that the el-ph interaction plays a secondary role¹. The fact that the undoped cuprates are Mott antiferromagnetic insulators supports the notion that strong Coulomb interactions are dominant and that the essential physics is contained in the Hubbard and t-J models². On the other hand, however, a variety of experiments also display pronounced phonon and electron-lattice effects in these materials: superconductivity-induced phonon renormalization³, large isotope coefficients away from optimal doping^{4,5}, tunneling phonon structures^{6,7}, etc., give evidence of significant el-ph coupling. Recently, photoemission data indicated a sudden change in the electron dispersion near a characteristic energy scale^{8,9}, which is possibly caused by coupling of electronic quasiparticles to phonon modes. Furthermore, neutron scattering data suggest that the oxygen half-breathing $(\pi, 0)$ phonon mode couples strongly to charge carriers and correspondingly, softens significantly with doping¹⁰.

To elucidate the effects of strong electronic correlations on the el-ph interaction, several authors have calculated the el-ph vertex function in the one- and three-band Hubbard models based on $(1/N)$ expansion within slave-boson^{11,12} and X operator¹³ formalisms. One finding¹³ is that for the ionic, i.e. onsite, el-ph coupling in the underdoped regime, the backward scattering with large phonon momentum transfer is suppressed much more than the forward scattering with small phonon momentum transfer. Based on this finding, it was argued that a forward peaking of the renormalized el-ph vertex could account for the absence of phonon features in the transport data. In addition, an el-ph interaction which is peaked at small phonon momentum transfer contributes to an attractive interaction in the $d_{x^2-y^2}$ -pairing channel^{13,14}. One should notice that these previous calculations were lim-

ited by the approximate nature of $1/N$ and slave-boson treatments, moreover, they were carried out for infinite U .

Here, we would like to use a more accurate numerical method to gain further insight into the way in which strong electron correlations dress the electron-phonon coupling for a range of values of U from weak to strong coupling. This analysis is important since it turns out that the U dependence of the electron-phonon coupling shows a dramatic change as a function of U (see below). Specifically, we apply the Determinantal Monte Carlo¹⁵ algorithm to find the single-particle response to external phonon fields in the one-band Hubbard model. In particular, we will calculate an effective el-ph coupling $g(p, q)$ (effective el-ph vertex) for scattering quasiparticles near the Fermi surface (which includes screening, vertex corrections, and the quasiparticle renormalization) produced by the Hubbard U .

Our calculations will be carried out at temperatures of order $\frac{1}{16}$ of the bandwidth ($W = 8t$) and for values of U which range up to the bandwidth. In this parameter regime, the renormalization of the el-ph coupling is determined by U . Our principle findings are: (1) Initially (up to the value of $U = 6$), as the Hubbard-Coulomb interaction U increases, the el-ph coupling is suppressed by electronic correlations for all phonon and electron momenta, and in particular for the backward scattering around $q = (\pi, \pi)$. (2) The behavior changes in the strong-coupling regime ($U > 6$). Here, the effective el-ph coupling at small phonon momentum transfer increases with increasing U , while the one at large phonon momentum transfer appears to saturate (see Fig. 3).

Our starting point is the one-band Hubbard model,

$$H = -t \sum_{\langle ij \rangle, \sigma} (c_{i\sigma}^\dagger c_{j\sigma} + c_{j\sigma}^\dagger c_{i\sigma}) + U \sum_i n_{i\uparrow} n_{i\downarrow}. \quad (1)$$

The operators $c_{i\sigma}^\dagger$ and $c_{i\sigma}$ as usual create and destroy an electron with spin σ at site i , respectively and the

sum $\langle ij \rangle$ is over nearest-neighbor lattice sites. Here, U is the onsite Coulomb interaction and we will choose the nearest-neighbor hopping t as the unit of energy.

In our simulations, we have used the linear-response technique to extract the el-ph vertex function. In this method, one formally adds to Eq. (1) the interaction,

$$H_{el-ph} = \sum_{kq\sigma} g_{kq}^0 c_{k+q\sigma}^\dagger c_{k\sigma} e^{-i\omega_m \tau}, \quad (2)$$

where g_{kq}^0 is the bare el-ph coupling. One then considers the response of the anomalous single particle propagator to this perturbation,

$$G_2(p, q) = - \int_0^\beta d\tau e^{i(\omega_n + \omega_m)\tau} \langle T_\tau c_{p+q\sigma}(\tau) c_{p\sigma}^\dagger(0) \rangle_{H+H_{el-ph}}, \quad (3)$$

where $\langle \rangle_{H+H_{el-ph}}$ stands for the Green's function evaluated with the Hamiltonian $H + H_{el-ph}$. The el-ph vertex function $\Gamma(p, q)$ is obtained by calculating the leading linear response of G_2 to H_{el-ph} , which is given by

$$G_2(p, q) = \int_0^\beta d\tau e^{i(\omega_n + \omega_m)\tau} \int_0^\beta d\tau' e^{-i\omega_m \tau'} \sum_{kq\sigma'} g_{kq}^0 \times \langle T_\tau C_{k+q\sigma'}^\dagger(\tau') C_{k\sigma'}(\tau') C_{p+q\sigma}(\tau) C_{p\sigma}^\dagger(0) \rangle_H \quad (4)$$

The two-particle Green's function in Eq. (4) is evaluated with respect to the pure Hubbard Hamiltonian in Eq. (1) and p and q stand for both the momentum and Matsubara frequencies ($\mathbf{p}, i\omega_n$) and ($\mathbf{q}, i\omega_m$), respectively. Diagrammatically $G_2(p, q)$ has the structure shown in Fig. 1 so that $\Gamma(p, q)$ can be written as

$$\Gamma(p, q) = \frac{G_2(p, q)}{G(p+q)G(p)} \quad (5)$$

Here, Γ is the el-ph vertex containing full contributions from Coulomb interactions only¹⁶. Close to the Fermi energy, the single-particle Green's function can be written as

$$G(p) = \frac{1}{Z(p)(i\omega_n - E_{\mathbf{p}})}. \quad (6)$$

where $Z(p)$ is the wave-function renormalization and $E_{\mathbf{p}}$ the quasiparticle excitation energy. Then for electron scattering processes which involve states near the Fermi surface, the effective el-ph coupling reads

$$g(p, q) = \frac{\Gamma(p, q)}{\sqrt{Z(p)Z(p+q)}} \quad (7)$$

Thus, we proceed as follows: a Monte Carlo calculation of $G_2(p, q)$ along with $G(p)$ and $G(p+q)$ is carried out. Then $Z(p)$ and $Z(p+q)$ are extracted from the single particle Green's functions. Finally, we obtain the effective el-ph coupling $g(p, q)$ from Eq. (7).

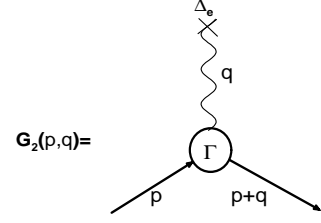


FIG. 1: Diagrammatic representation of $G_2(p, q)$ within linear response to g_{kq}^0 . The thick solid lines represent dressed single-particle Green's functions of the Hubbard model. The wavy line denotes the external perturbation in Eq. (2).

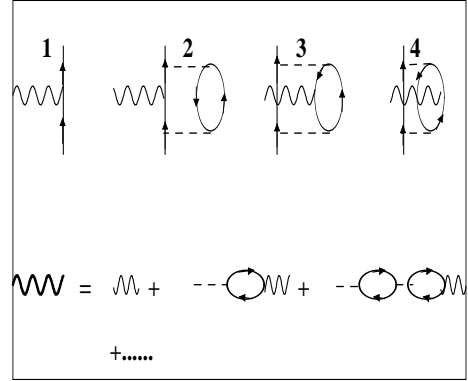


FIG. 2: Low-order Feynman diagrams for the irreducible el-ph vertex $\Lambda(p, q)$ (top) and low-order polarization graphs (lower) that enter the full vertex Γ . The thin solid lines are the non-interacting Green's functions and the dashed lines represent the Hubbard interaction U . The thin (thick) wavy line stand for the bare (screened phonon) fields.

In the following, we will focus on the case of an *ionic* el-ph coupling, in which the bare coupling g_{pq}^0 is a constant g^0 . Since we are considering linear terms in g^0 only, we can set g^0 equal to 1. This corresponds to the simple Holstein form of the el-ph interaction, which is an important limiting case. Moreover, having the bare interaction independent of p and q makes it easier to see modifications, which arise from the strong U correlation effects.

The low order U and U^2 vertex contributions to Γ are displayed in Fig. 2. The diagrams shown at the bottom of Fig. 2 are the leading terms of the RPA approximation $(1 - \frac{1}{2} U \Pi_0(q))^{-1}$ to the polarization correction, with $\Pi_0(q)$ the contribution from the single bubble. The exact Monte Carlo result for the polarization correction is $1 + \frac{1}{2} U \Pi(q)$ with

$$\Pi(q) = - \int_0^\beta d\tau e^{-i\omega_m \tau} \langle T_\tau \rho_q(\tau) \rho_q^\dagger(0) \rangle$$

and

$$\rho_q^\dagger = \frac{1}{\sqrt{N}} \sum_{k\sigma} c_{k+q\sigma}^\dagger c_{k\sigma}. \quad (8)$$

With this in mind, Γ can be written in terms of the screening factor and an irreducible vertex $\Lambda(p, q)$, which is the sum of graphs that can not be separated into two pieces by cutting a single dashed Coulomb interaction line U (see Fig. 2), *i.e.*

$$\Gamma(p, q) = (1 + \frac{1}{2}U\Pi(q))\Lambda(p, q). \quad (9)$$

Thus, the strong-coupling effects associated with the Hubbard-Coulomb interaction U lead to an effective el-ph coupling which can be expressed in the canonical form

$$g(p, q) = \frac{(1 + \frac{1}{2}U\Pi(q)) \Lambda(p, q)}{(Z(p)Z(p+q))^{\frac{1}{2}}} \quad (10)$$

and one sees that it consists of a product of an irreducible vertex $\Lambda(p, q)$, a screening factor $(1 + \frac{1}{2}U\Pi(q))$, and a quasiparticle renormalization $(Z(p)Z(p+q))^{-\frac{1}{2}}$ factor.

Our numerical Monte Carlo simulations were performed on an 8×8 lattice at an inverse temperature $\beta = 2$ and a filling $\langle n \rangle = 0.88$. We have set the frequencies to their minimum values, *i.e.*, $\omega_n = \pi T$ for fermions and $\omega_m = 0$ for bosons. While we are interested in low-frequency scattering processes, it is not clear whether one can correctly extrapolate to the $\omega_n \rightarrow 0$ limit from the lowest accessible fermionic Matsubara frequency $\omega_n = \pi T$ at high temperatures. For this reason, we have checked some special cases for which one can reach lower temperatures, namely a 2D system at weak coupling and/or with large doping ($\langle n \rangle = 0.65$). For these systems, we have found that the real part of the vertex function $\Gamma(\mathbf{p}, i\pi T, \mathbf{q}, 0)$ depends only weakly on temperature, and the imaginary part always vanishes as $T \rightarrow 0$. In the following we will, therefore, focus on the real part of the vertex function at the lowest fermionic Matsubara frequency. To test the accuracy of our technique, which involves the Trotter approximation and the τ integrations, we have compared Monte Carlo results with the results from exact diagonalization on a 4-site ring. The comparison demonstrates that the QMC calculations are very accurate for the scattering process that we have studied.

We are interested in el-ph scattering processes in which the incoming and the outgoing electron momenta \mathbf{p} and $\mathbf{p} + \mathbf{q}$ are close to the Fermi surface. For an 8×8 lattice doped near half-filling, the q and U dependence of $g(p, q)$ for the scattering processes on the half-filled diamond Fermi surface is studied. In particular, we will examine initial states corresponding to $\mathbf{p} = (-\pi, 0)$ and $\mathbf{p} = (-\pi/2, \pi/2)$. Other choices of \mathbf{p} and $\mathbf{p} + \mathbf{q}$ close to the half-filled diamond Fermi surface give qualitatively similar results to those reported here.

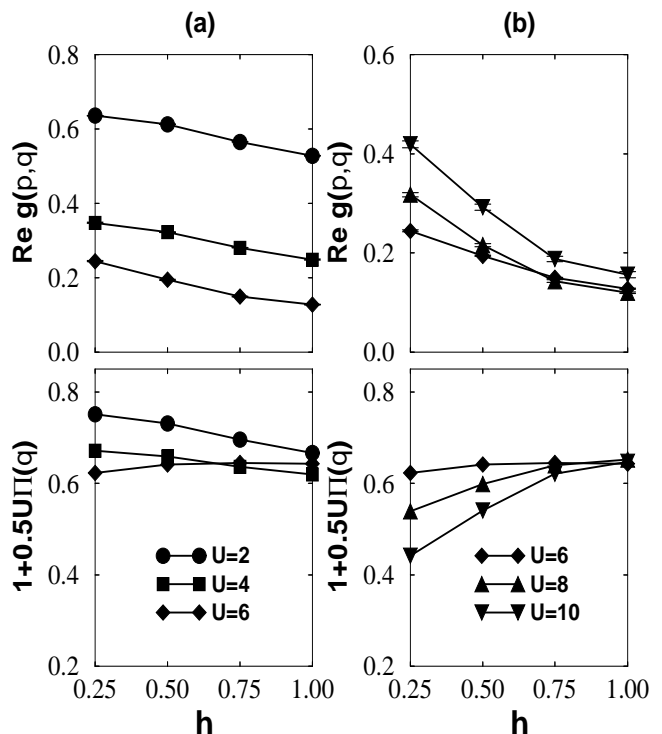


FIG. 3: Real part of the effective el-ph coupling $g(p, q)$ and the polarization factor $1 + \frac{1}{2}U\Pi$ versus \mathbf{q} for (a) $U \leq 6$ and (b) $U \geq 6$. Here $\mathbf{q} = \pi(h, h)$ with h the tick label of the x axis. The incoming electron carries momentum $\mathbf{p} = (-\pi, 0)$ and the value of U is indicated by the shape of the symbol.

Monte Carlo results for $g(p, q)$ and for the polarization factor $(1 + \frac{1}{2}U\Pi)$ are shown in Fig. 3. The left hand side, Fig. 3a, shows the behavior in the weak- and intermediate-coupling regimes. The right hand side of the figure, Fig. 3b, shows similar results when the system enters the strong-coupling regime. One can clearly see that when the Hubbard U is smaller than $U \approx 6$, $g(p, q)$ decreases as a function of U from its bare value $g^0 = 1$, for all momentum transfers. Then, as the interaction U increases to the strong-coupling case ($U \sim W$), the effective el-ph coupling begins to increase. This behavior is particularly evident at smaller values of momentum transfer. In the strong-coupling regime, the overall q dependence of the el-ph coupling agrees reasonably well with the results of the $1/N$ expansion¹³ which are obtained for the $U \rightarrow \infty$ limit. However, in our case the interesting behavior is that the effective el-ph coupling as a function of U is nonmonotonic, first decreasing and then, at physically interesting values of U , increasing. This finding deviates from the prediction of a Fermi-liquid analysis¹². According to this analysis, $g(p, \frac{i\omega_m}{\mathbf{q}} \rightarrow 0) \propto \frac{1}{1+F_0^s}$ with F_0^s the zero-harmonic symmetric Landau amplitude so that the effective el-ph coupling decreases monotonically with increasing U since F_0^s becomes larger with U .

From Fig. 3, one can see that the polarization fac-

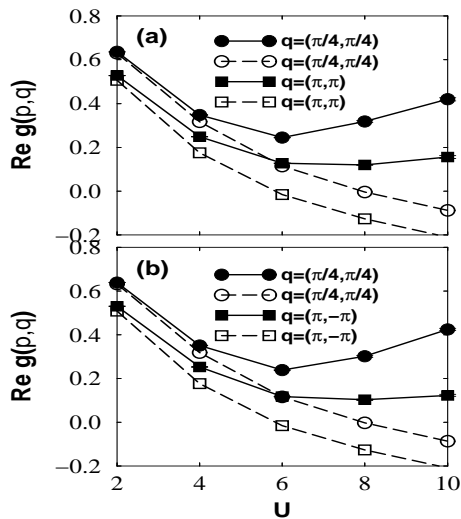


FIG. 4: Real part of $g(p, q)$ as a function of U for (a) $\mathbf{p} = (-\pi, 0)$ and (b) $\mathbf{p} = (-\pi/2, \pi/2)$. The value of q is indicated by the shape of the symbol. The solid circles are Monte Carlo results and the open symbols show the perturbation theory contributions shown in Fig. 2.

tor acts quite generally to suppress the el-ph coupling. At large momentum transfer, this quantity saturates as U increases, while at small momentum transfer it continues to decrease due to the increase of $|\Pi(q)|$. Comparison between $g(p, q)$ and the polarization factor indicates that at weak-coupling screening is the dominant correlation effect suppressing the el-ph coupling. On the other hand, with an increasing Hubbard U , the vertex corrections Λ become more important, making the effective el-ph coupling peaked in the forward scattering direction. At present, we only have a qualitative understanding of the physical mechanism responsible for the increase of effective el-ph coupling in the strong-coupling case. Considering the fact that the ionic el-ph vertex is largely determined by the density fluctuation spectrum, which depends crucially on the electronic structure of the strongly correlated electron system, this increase of $g(p, q)$ as a function of U can be attributed to the renor-

malization of the low-energy single-particle and charge excitations from the t - to the $J = \frac{4t^2}{U}$ -scale upon entering the strong-coupling regime.

In order to see the U dependence more clearly, in Fig. 4 Quantum Monte Carlo calculations are compared with perturbation theory for different values of U . Here, the solid symbols are Monte Carlo results and the open symbols show the results obtained by evaluating $\Gamma(p, q)$ perturbatively with the diagrams of 2. In the perturbative calculations, $g(p, q)$ is calculated by using wave-function renormalizations $Z(p)$ and $Z(p+q)$ extracted from Monte Carlo data. As one can see, in the weak-coupling regime, the perturbative calculations are in good agreement with Monte Carlo simulations. However, when the Hubbard U exceeds $U \approx 4$ ($\sim \frac{W}{2}$), perturbation theory appears to break down.

In summary, based on QMC simulations, we have studied the el-ph vertex function in the two-dimensional Hubbard model. We find that in the weak-coupling regime, the effects of the Hubbard interaction U are to *suppress* the ionic el-ph coupling at all phonon momenta, with backward scattering processes being more strongly suppressed than forward ones. On the other hand, in the strong-coupling regime, the vertex at smaller phonon momentum transfer anomalously *increases* as a function of U . We also find that screening is the dominant contribution to the vertex corrections at weak-coupling, while at strong-coupling the irreducible vertex corrections are crucial.

We would like to acknowledge useful discussions with Dr. R. Zeyher and C. Castellani. The Würzburg group would like to acknowledge support by the DFG under Grant No. Ha 1537/16-2 and by a Heisenberg fellowship (AR 324/3-1), and by the Bavaria California Technology Center (BaCaTeC), the KONWHIR projects OOPCV and CUHE. DJS acknowledges support from the US Department of Energy under Grant #DOE85-45197. The calculations were carried out at the high-performance computing centers HLRS (Stuttgart) and LRZ (München).

¹ M. Imada, A. Fujimori, and Y. Tokura, *Rev. Mod. Phys.* **70**, 1039 (1998).

² P.W. Anderson; cond-mat/0201429.

³ V.G. Hadjiev, X.J. Zhou, T. Strohm, M. Cardona, Q.M. Lin, and C.W. Chu, *Phys. Rev. B* **58**, 1043 (1998); for a review, see also M.L. Kuclic, *Physics Reports* **338**, 1–264 (2000).

⁴ J.P. Frank, S. Harker, and J.H. Brewer, *Phys. Rev. Lett.* **71**, 283 (1993).

⁵ G.M. Zhao, H. Keller, and K. Conder; cond-mat/0204447,0204448.

⁶ D. Shimada, Y. Shiina, A. Mottate, Y. Ohyagi, and

N. Tsuda, *Phys. Rev. B* **51**, R16495 (1995).

⁷ R.S. Gonnelli, G.A. Ummarino, V.A. Stepanov, *Physica C* **275**, 162 (1997).

⁸ Z.X. Shen, A. Lanzara, S. Ishihara, and N. Nagaosa; cond-mat/0108381.

⁹ A. Lanzara, P.V. Bogdanov, X.J. Zhou, S.A. Keller, D.L. Feng, E.D. Lu, T. Yoshida, H. Eisaki, A. Fujimori, K. Kishio, J.-I. Shimoyama, T. Noda, S. Uchida, Z. Husain, and Z.-X. Shen, *Nature* **412**, 510 (2001).

¹⁰ R.J. McQueeney *et al.*, *Phys. Rev. Lett.* **82**, 628 (1999); Y. Petrov, T. Egami, R.J. McQueeney, M. Yethiraj, H.A. Mook, and F. Dogan; cond-mat/0003414.

- ¹¹ J.H. Kim, K. Levin, R. Wentzconvitch, and A. Auerbach, *Phys. Rev. B* **44**, 5148 (1991); J.H. Kim, and Z. Tesanovic, *Phys. Rev. Lett.* **71**, 4218 (1993).
- ¹² M. Grilli and C. Castellani, *Phys. Rev. B* **50**, 16880 (1994).
- ¹³ R. Zeyher and M. Kubic, *Phys. Rev. B* **53**, 2850 (1996).
- ¹⁴ N. Bulut and D.J. Scalapino, *Phys. Rev. B* **54**, 14971 (1996).
- ¹⁵ R. Blankenbecker, D.J. Scalapino, and R.L. Sugar, *Phys. Rev. D* **24**, 2278 (1981).
- ¹⁶ This method could, of course, be extended to take into account phonon vertex corrections, but here we are interested in understanding the effects of the Hubbard interaction U on the vertex.